

The Corrosion and Wear Performance of Microcrystalline WC-10Co-4Cr and Near-Nanocrystalline WC-17Co High Velocity Oxy-Fuel Sprayed Coatings on Steel Substrate

GOBINDA C. SAHA and TAHIR I. KHAN

The study of near-nanocrystalline cermet composite coating was performed by depositing near-nanocrystalline WC-17Co powder using the high velocity oxy-fuel spraying technique. The WC-17Co powder consists of a core with an engineered near-nano-scale WC dispersion with a mean grain size 427 nm. The powder particle contains 6 wt pct of the ductile phase Co matrix mixed into the core to ensure that the reinforcing ceramic phase WC material is discontinuous to limit debridement during wear, while the remainder of the binding phase (11 wt pct) is applied as a coating on the powder particle to improve the ductility. The tribological properties of the coating, in terms of corrosion resistance, microhardness, and sliding abrasive wear, were studied and compared with those of an industrially standard microcrystalline WC-10Co-4Cr coating with a WC mean grain size 3 μm . Results indicated that the WC-17Co coating had superior wear and corrosion resistance compared to the WC-10Co-4Cr coating. The engineered WC-17Co powder with a duplex Co layer had prevented significant decarburization of the WC dispersion in the coating, thereby reducing the intersplat microporosity necessary for initiating microgalvanic cells. The improved wear resistance was attributed to the higher hardness value of the near-nanocrystalline WC-17Co coating.

DOI: 10.1007/s11661-010-0296-1

© The Minerals, Metals & Materials Society and ASM International 2010

I. INTRODUCTION

WEAR and corrosion are two major concerns affecting the operational life of machinery and equipment engaged in bitumen conversion in oil sands operations. Thermally sprayed cermet coatings are well established for providing high hardness, wear, and corrosion resistant surfaces with a low coefficient of friction.^[1-3] Wide use of tungsten carbide based cermet coatings has been documented leading to wear resistance in several industrial applications including cutting tools and mining bits; teeth on gravel extractors and similar earth moving equipment; mineral, pulp, and paper processing; aerospace and automobile manufacturing; and power generation.^[4-6] Hard coatings deposited by thermal spraying of conventional microcrystalline WC-10Co-4Cr, an industrially standard cermet powder, by high velocity oxy-fuel (HVOF) technique have shown better results when used to protect against abrasive environments compared with hardfacing of surfaces by fusion welding techniques or heat treatments.^[7] The HVOF sprayed WC-Co coatings with a near-nanometer scale WC grain size with superior wear and corrosion resistant properties have yet to exploit their full potential in oil sands applications.^[8-10]

There are many kinds of cermet powders that are commercially available and are produced by several different manufacturing methods, including cast crushed, sintered crushed, agglomerated, aggregated, and coated. Nanocrystalline WC-Co powders have been successfully fabricated in large quantities using thermo-mechanical techniques and mechanical milling processes.^[11-14] While the reported result^[15-18] links nanometer range WC grain size with increased hardness and resistance to abrasive and sliding wear of sintered, bulk, WC-Co composites, many have found a disappointing sliding and abrasive wear resistance of nanocrystalline WC-Co coatings deposited with powders that are prepared with the spray-dry process.^[15,19,20] The latter has identified increased decarburization of the coatings as the origin of their disappointing performance. A quantitative review of the influences of spray process and powder properties on the tribological performance of the thermal sprayed WC-Co coatings has further confirmed this tendency.^[21] Therefore, it was believed that the achievement of superior wear and material performance from nanocrystalline coatings would require an optimization of the powder manufacturing and a readaptation of the spray process.^[22-26]

Coatings are most often applied to improve corrosion and wear resistance. However, neither corrosion nor wear takes on a singular form,^[27] and they often occur simultaneously. This indicates the importance of choosing the best coating material for a specific application. In this research, an engineered near-nanocrystalline metal clad WC-17Co cermet powder was used. The novelty is that the powder particles are engineered so as

GOBINDA C. SAHA, Research Associate, and TAHIR I. KHAN, Professor, are with the Department of Mechanical & Manufacturing Engineering, The University of Calgary, Calgary, Alberta T2N 1N4, Canada. Contact e-mail: tkhan@ucalgary.ca

Manuscript submitted November 2, 2009.

Article published online July 13, 2010

to determine where the ductile phase is without modifying the overall composition of the powder. Figure 1 shows a schematic comparing a typical spray-dried WC-17Co particle and an engineered particle with the same composition.

The engineered particle contains Co (*i.e.*, ductile phase) 6 wt pct mixed into the core to ensure that the WC reinforcement phase is dispersed discontinuously to limit debondment during wear. The remainder of the binding phase (11 wt pct) is applied as a coating on the particle to improve ductility of the sprayed coating. Furthermore, a near-nanocrystalline WC size was used, because it provides a smaller surface area to volume ratio, thereby having a lower tendency toward decarburization than many commercially available nanocrystalline WC powders. The decarburization of WC leads to the formation of graphite, which readily oxidizes in the presence of oxygen to CO₂. This results in porosity within the coating, which, in turn, results in poor mechanical and corrosion resistant properties.

The objective of this article was to evaluate the differences in the corrosion and wear resistant behavior of an industrially used microcrystalline WC-10Co-4Cr coating and a novel duplex near-nanocrystalline WC-17Co coating as a potential replacement for abrasive wear and corrosion resistance. The changes in the tribological properties of these coatings are explained in terms of microstructural developments during the HVOF spraying process.

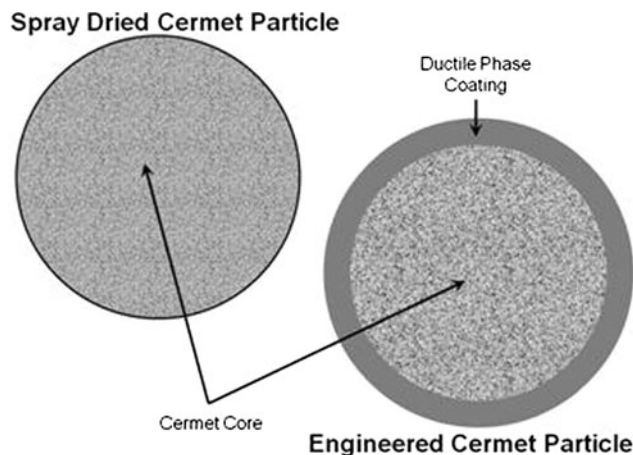


Fig. 1—Schematic comparing a traditional spray-dried cermet powder and engineered cermet particle.^[28]

II. EXPERIMENTAL PROCEDURE

A. Material

Two different powders were used as feedstock in this study: near-nanocrystalline WC-17Co and conventional microcrystalline WC-10Co-4Cr (provided by Sulzer Metco, Westbury, NY). Table I shows the results from a chemical analysis of the powders carried out using a Noran 8-channel energy dispersive spectroscope (Noran Instruments, Middleton, WI).

The near-nanocrystalline WC-17Co powder was obtained from MesoCoat Inc. (Euclid, OH). The manufacturing method for producing the near-nanocrystalline WC-17Co powder consisted of powder precursor acquisition, milling, spray drying, debinding, sintering, and particle sizing. The precursor powder was milled to attain the desired particle characteristics and chemical balance. The milled powder was then spray dried resulting in a raw blended powder with a relatively narrow size distribution (Figure 2(a)). The spray-dried powder was collected, debound, and sintered to remove any residuals from the milling and spray drying processes. Once the material was removed from the furnace, it was then ground and sifted to the required size in preparation for coating by chemical vapor deposition (CVD). The CVD coating process was used to develop a thin coating around the individual powder particles resulting in a Co coated near-nanocrystalline powder (Figure 2(b)). Using a combination of sifting and sedimentation techniques, the powder was sized to meet the user requirement and final scanning electron microscopy (SEM) was performed, as shown in Figure 2(c). A particle size analysis was performed for quality assurance (Figure 2(d)). The micrograph shows that the near-nanocrystalline WC-17Co powder had a spherical morphology, which was superficially indifferent to the traditional microcrystalline WC-10Co-4Cr powder (Figure 2(e)). From Figure 2(d), it is seen that the particle size distribution of the near-nanocrystalline powder was near Gaussian with a range from 0.5 to 50 μm.

C-Mn grade AISI 1018 steel substrates were employed because of the wide industrial use of this low cost material. The annealed AISI 1018 steel had a nominal chemical composition (in wt pct): 0.18-C, 0.16-Si, 0.65-Mn, and balance Fe. Two different geometries of this material were used as substrates: (a) flat plate (100 × 25 × 12 mm) and cylindrical rod (6.30-mm o.d. × 10-mm height). After machining, the surfaces had an average surface roughness parameter R_a (according to UNI ISO 4287/1 definition) value of 0.81 μm. The surfaces were prepared for spraying by grit blasting on

Table I. Chemical Composition of Coating Powders

Characteristic	Powder	
	Engineered Near-Nanocrystalline WC-17Co	Microcrystalline WC-10Co-4Cr
Element, wt pct	balance W, 18.5-Co, 5.6-C, 1.11-O	balance W, 10-Co, 5-C, 4-Cr, 1-others
Manufacturing route	clad	agglomerated/sintered
Particle shape	mostly spherical	mostly spherical

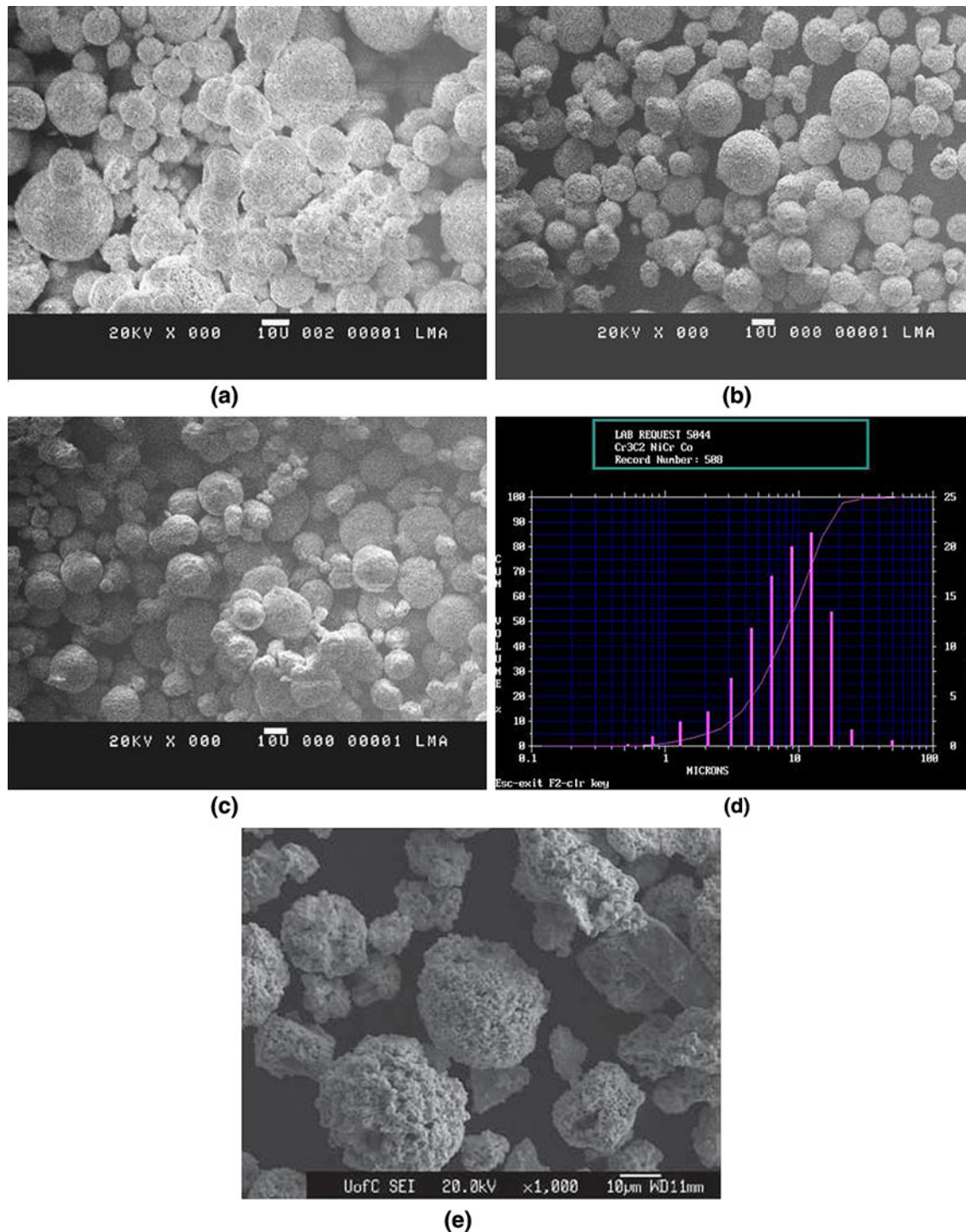


Fig. 2—Scanning electron micrograph showing near-nanocrystalline WC-17Co particle after (a) milling and spray drying; (b) debinding, sintering, and CVD coating; (c) sizing; (d) microtrack graph showing particle size distribution; and (e) morphology of microcrystalline WC-10Co-4Cr particle.

one side with a 97 pct Al_2O_3 and 3 pct TiO_2 mixture using a 686- μm grit size. The specimens were degreased with acetone followed by cleaning in an ultrasonic bath. The mean surface roughness, R_a , was measured at $11 \pm 2 \mu\text{m}$. The HVOF spraying was carried out at Hyperion Technologies Inc. (Calgary, AB), using the conditions specified in Table II.

The ratio between methane to oxygen in the fuel mixture was maintained at 0.68 to create an optimum crystalline phase structure within the final coating. A transverse spraying speed of 0.2 m/s was used to obtain approximately 5- μm thickness per pass. A coating thickness gage (3000FX model) was used, and a coating thickness measurement was performed according to

ASTM E376-06; the final coating thickness was measured to be 529 μm .

B. Characterization

The corrosion tests consisted of working electrodes, which were made of the coated and uncoated AISI 1018 carbon steel strips (10 \times 5 \times 4 mm) axially embedded in Araldite holders to an exposed area of 0.25 cm^2 to the test solution. The top surface of the specimen was ground on SiC papers and polished to a mirror finish using 1- μm Al_2O_3 powder. The electrodes were ultrasonically cleaned with ethanol, washed with distilled water, and then covered with epoxy on all sides with the top surface exposed for the test solution. The test specimen was then introduced into a deaerated test solution composed of 0.86 M (3.5 wt pct) NaCl solution, at room temperature 299 K (\sim 26 $^\circ\text{C}$). The choice of test solution was based on earlier work done to study the corrosion behavior of WC/Co coating systems.^[2,29] A platinum wire was used as the counter electrode and all potentials were measured against a standard calomel electrode (SCE). To avoid contamination, the reference electrode was connected to the working electrode through a bridge with a Luggin capillary filled with the test solution. The capillary tip was positioned within 1 mm of the electrode surface to minimize the ohmic drop of the solution.

The aqueous corrosion behavior of the specimens was studied using both polarization and electrochemical impedance techniques. Electrochemical measurements were performed on a three-electrode cell through a Solartron 1280C electrochemical measurement system (Calgary, AB, Canada). Prior to electrochemical measurements, the electrode was immersed in the test solution for 4 hours until the steady-state corrosion potential was reached. A potentiodynamic polarization curve was measured by potential scanning 600 mV above and below the corrosion potential of -0.6 V using an open circuit potential at a sweep rate of 1 mV/s. Infrared compensation was applied through the instrument. Electrochemical impedance spectroscopy (EIS) was measured with a sinusoidal potential excitation of 10 mV amplitude in the frequency range from 20 kHz to 10 mHz at corrosion potential. The surface morphology and composition of the surface scale were observed and analyzed by SEM and energy-dispersive X-ray analysis (EDXA), respectively.

Table II. Spraying Conditions Adopted for HVOF Spraying Process

Condition	Parameter
HVOF process spray gun	Diamond Jet 2700 with water cooling
Fuel gas	O_2 -1346 slpm,* CH_4 -918 slpm, shroud gas (air)-1742 slpm
Carrier gas	N_2 -60 slpm
Spraying distance	23 cm
Powder feeder type	9MPDJ
Feed rate	38 g/min

*Standard liter per minute.

For mechanical characterization as well as abrasive wear testing of the coatings, the surfaces of all other specimens were prepared by polishing to a 1- μm finish. Specimens were etched using a mixture of 1 to 2 parts KOH (10 pct aqueous) with 1 part $\text{K}_3\text{Fe}(\text{CN})_6$ (10 pct aqueous) solution. The scanning electron microscope used was a JSM-8200 Multiprobe JEOL* in the

*JEOL is a trademark of Japan Electron Optics Ltd., Tokyo.

backscattered mode under conditions of contrast to enhance features such as porosity. The phases present within the coatings were determined by X-ray diffraction (XRD) analysis using Rigaku Multiflex (Tokyo, Japan). A Cu K_α radiation source with a step size of 0.1 deg, a step time of 1 second, and a 2θ scan window from 25 to 55 deg was used. The hardness values of the coatings were determined using a microhardness tester (Micro-met II, Buehler, Calgary, AB, Canada) equipped with a Vickers diamond pyramid indenter operating under 300 g load.

The abrasive wear behavior of the coatings was assessed using a two-body abrasive wear test performed on a pin-on-disc apparatus with a load of 1.0 kg. The specimen represented the pin and the disk was a 120 grit size SiC grinding paper attached to the reciprocating table of the wear testing machine. A total sliding distance of 320 m and a speed of 5.34 m/min were used for the wear tests. The SiC paper was changed every 40 m distance completed so that fresh abrasives were exposed to the test surface.

III. RESULTS AND DISCUSSION

A. XRD Analysis of the Coatings

The microstructure of C-Mn steel is shown in Figure 3. The steel consists of ferrite grains of approximately 20- μm size with pearlite colonies. The microstructures of the coatings were examined using SEM,

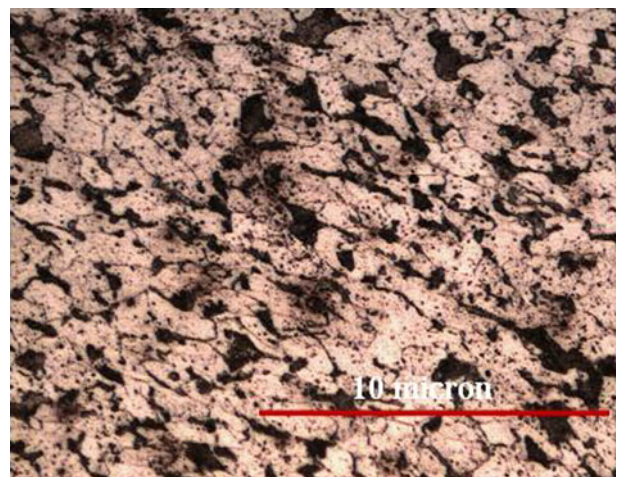
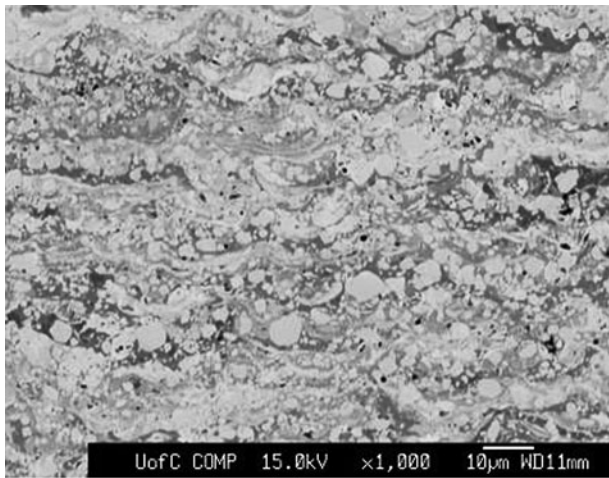
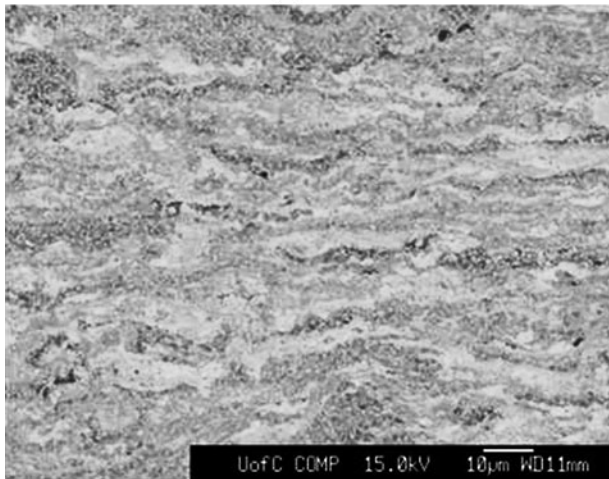


Fig. 3—Light micrograph showing the microstructure of AISI 1018 carbon steel.



(a)



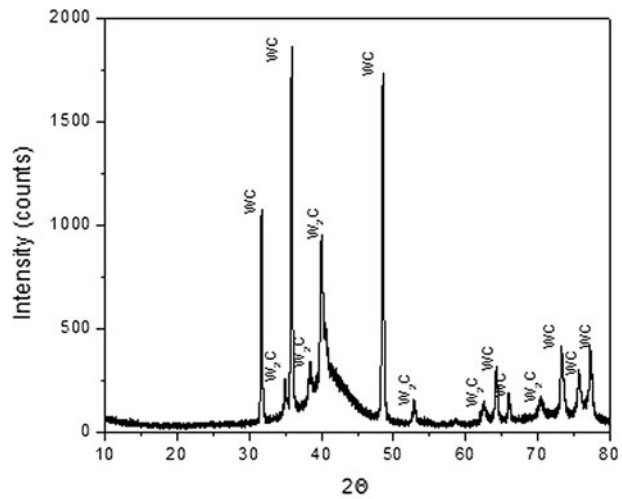
(b)

Fig. 4—SEM micrographs showing (a) microcrystalline WC-10Co-4Cr and (b) near-nanocrystalline WC-17Co coating surfaces.

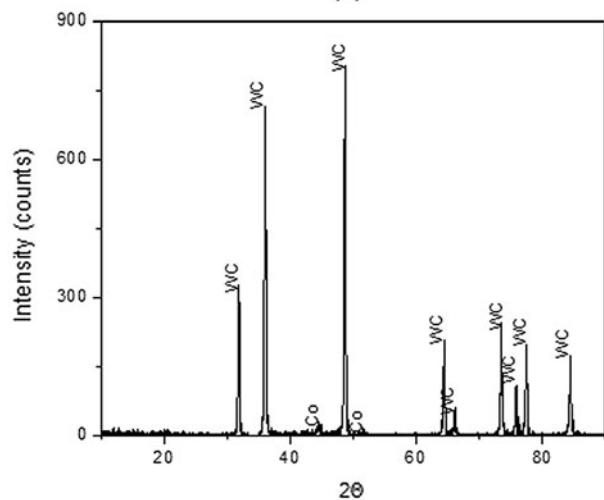
and the micrographs of the microcrystalline and near-nanocrystalline as-sprayed coatings were shown in Figure 4.

It is evident that the engineered near-nanocrystalline coating (Figure 4(b)) contains a finer dispersion of WC grains compared with the traditional microcrystalline WC-10Co-4Cr coating (Figure 4(a)). This is related to the fact that the engineered powder used in this study had a mean WC grain size of 427 nm, making the coating a near-nanocrystalline coating, whereas the conventional microcrystalline powder particle size ranged from 15 to 35 μm with a WC grain size of 1 to 3 μm . The near-nanocrystalline coating showed a dense coating, which was free from internal porosity and well-bonded WC particles. XRD analysis of the microcrystalline WC-10Co-4Cr coating showed the presence of W_2C in the sprayed coating suggesting that some decarburization of the WC occurred (Figure 5(a)).

Contrary to earlier published research,^[30,31] XRD analysis of the near-nanocrystalline coating showed no evidence of W_2C phase formation (Figure 5(b)). This suggested that extensive decarburization of WC during



(a)



(b)

Fig. 5—XRD analysis of (a) microcrystalline WC-10Co-4Cr and (b) near-nanocrystalline powders after spraying.

the spraying of the powder may have been prevented due to the use of the duplex Co coated WC-17Co powder used in this research. It is suggested that the duplex Co coating surrounding the WC core absorbed the latent heat of fusion, thus preventing an excessive increase in the temperature of the inner section of the powder particles where the near-nanocrystalline WC ceramic dispersion is located.

B. Corrosion Resistance

Figure 6 shows the time dependence of corrosion potential of coated and uncoated AISI 1018 steel. It can be seen that the corrosion potential for the bare carbon steel substrate was about -0.62 V (SCE). With the conventional microcrystalline WC-10Co-4Cr coating, the corrosion potential shifted to a more positive value of -0.59 V (SCE). For the near-nanocrystalline coating, the corrosion potential shifted to an even more positive value of -0.55 V (SCE). These results indicated that

both the microcrystalline and near-nanocrystalline coatings provided protection to the substrate and that the protection provided by the near-nanocrystalline coating was greater than the traditional microcrystalline coating.

The polarization curves recorded on AISI 1018 carbon steel, microcrystalline WC-10Co-4Cr, and near-nanocrystalline WC-17Co coatings under stagnant conditions are shown in Figure 7.

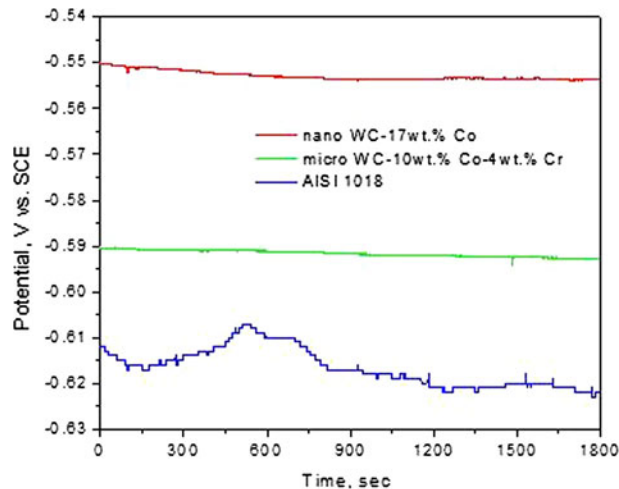


Fig. 6—Time dependence of corrosion potential of engineered WC-17Co, microcrystalline WC-10Co-4Cr coatings, and uncoated carbon steel in 3.5 wt pct NaCl solution.

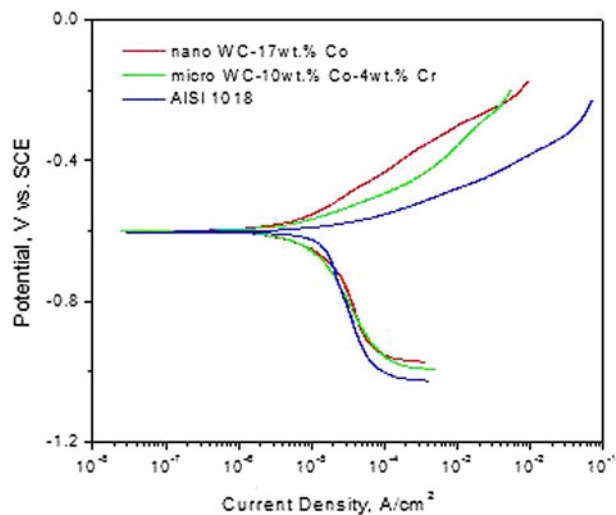


Fig. 7—Polarization curves for the WC-17Co, microcrystalline WC-10Co-4Cr coatings and uncoated carbon steel in 3.5 wt pct NaCl solution.

It is seen that both coatings inhibited the anodic current densities prominently, while the cathodic current densities were not affected significantly. The inhibition of anodic current density resulted in a positive shift of the corrosion potentials. There are limited current densities in the cathodic branch, which indicates that the cathodic reaction is a diffusion-controlled process regardless of whether the substrate is covered with the coatings. The values of the corresponding kinetic parameters in polarization curves such as corrosion potential (E_{corr}), corrosion current density (i_{corr}), and anodic and cathodic Tafel slope (b_a , b_c) are listed in Table III.

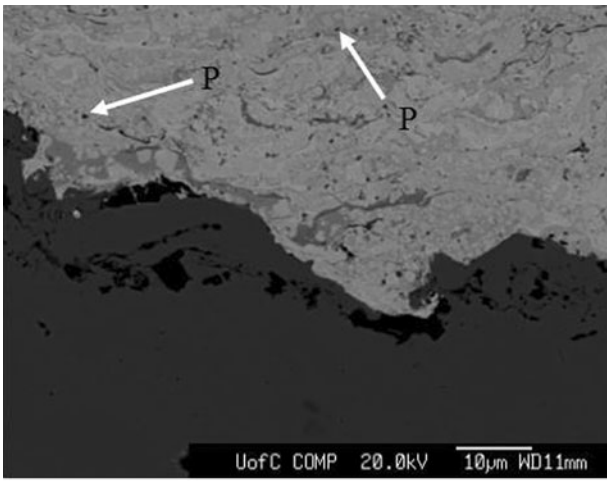
These kinetic parameters are obtained by performing linear fitting in the Tafel region of the measured data. From Figure 7 and Table III, it can be seen that the corrosion potential of coated electrodes is more positive than that of uncoated AISI 1018 electrode. The corrosion current density of the uncoated electrode was the largest, while the smallest corrosion current density was observed in the electrode with the engineered WC-17Co coating. The anodic Tafel slope of the uncoated electrode was smaller than those of coated electrodes, which indicated that the coatings inhibit the anodic process at the electrode. High cathodic Tafel slopes are obtained through fitting, which suggest that there is a diffusion-controlled cathodic process in place.

Figure 8 shows the scanning electron micrographs taken from the transverse sections of the coatings after subjecting the coatings to a potentiodynamic test in 3.5 wt pct NaCl solution. Examination of the surface of the coatings and the interface between the coat and steel substrate did not reveal any corrosive attack. However, a comparison of the microcrystalline and engineered near-nanocrystalline coatings after the corrosion test revealed microporosity (arrows marked “P” in Figure 8(a)) within the microcrystalline coating. This microporosity was not seen in the as-sprayed coating and suggested that dissolution of the coat metal matrix could be occurring due to corrosion. The EDXA spectrum of chemical composition of the coatings is shown in Figure 9. The specimens were coated with gold (also traced in the spectrum) for the purpose of electrical conductivity on the coated surfaces. From Figure 9(a), it is seen that a thicker layer of corrosion product formed on the traditional WC-10Co-4Cr electrode surface.

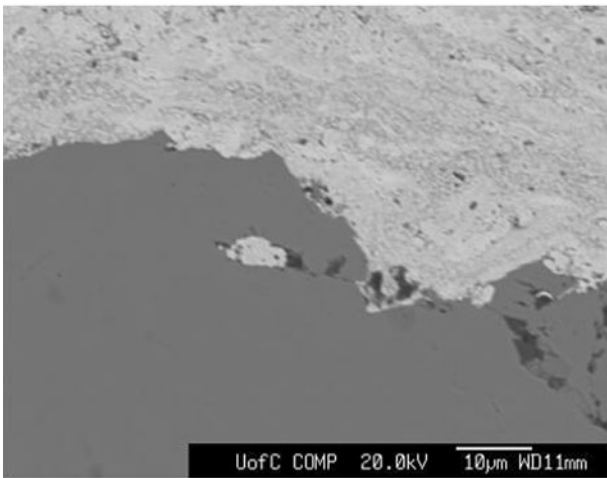
The results of the potentiodynamic test, shown in Figure 7, suggest that there was a noticeable difference in the anodic polarization curves obtained from the microcrystalline and near-nanocrystalline coatings. These correspond to an increase in ionic dissolution in the conventional microcrystalline coating and less in the engineered near-nanocrystalline coating. Earlier research by Perry *et al.*^[29] has shown that microgalvanic

Table III. Fitting Results of Electrochemical Parameters

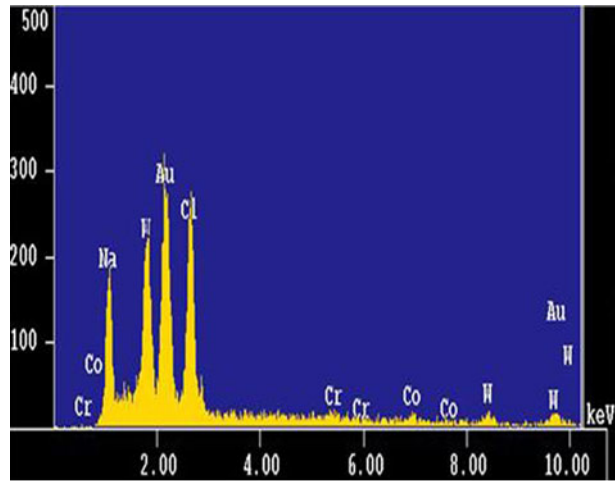
Specimen	Anodic b_a , mV _{SCE} /Dec	Cathodic b_c , mV _{SCE} /Dec	Current Density, A/cm ²	Potential, V _{SCE}
AISI 1018 steel	80.93	-545.88	3.02×10^{-5}	-0.602
Microcrystalline WC-10Co-4Cr	120.62	-409.71	1.50×10^{-5}	-0.601
Near-nanocrystalline WC-17Co	138.17	-572.05	6.08×10^{-6}	-0.584



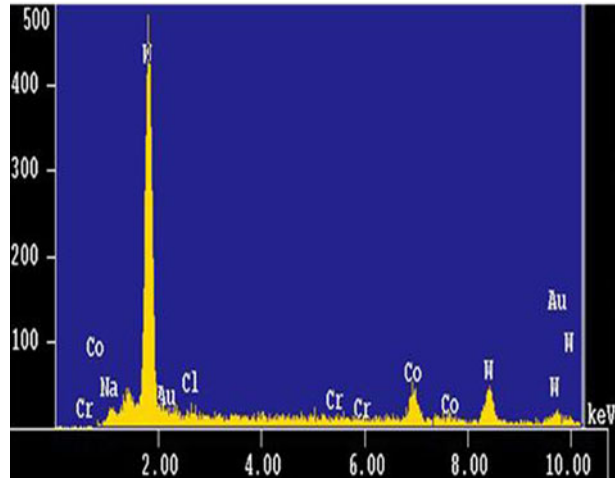
(a)



(b)



(a)



(b)

Fig. 8—SEM micrographs showing the interface between (a) microcrystalline WC-10Co-4Cr and (b) near-nanocrystalline WC-17Co coating and substrate.

Fig. 9—EDXA spectra taken from the surfaces of (a) microcrystalline WC-10Co-4Cr and (b) near-nanocrystalline WC-17Co coatings.

cells can form between the Co-Cr metal matrix and the WC particles resulting in localized dissolution and pore formation. Furthermore, these microgalvanic cells could be made worse by the decarburization of WC to W_2C , which forms throughout the microcrystalline WC-10Co-4Cr coating and was confirmed by XRD analysis, as shown in Figure 5(a). On the other hand, the engineered near-nanocrystalline WC-17Co coating produced a more refined and compact structure, thereby reducing intersplat microporosity necessary for initiating microgalvanic cells. However, the difference in Co content between the microcrystalline and near-nanocrystalline coatings may also contribute to the lower current density and higher charge transfer resistance shown by the near-nanocrystalline coating.

Figure 10 shows the Nyquist diagrams of coated and uncoated AISI 1018 steel substrate in 3.5 wt pct NaCl solution. From Figure 10, the impedance spectra of coated and uncoated electrodes emerge as capacitive semicircles at whole frequency. The diameter of the EIS semicircle, *i.e.*, the charge transfer resistance, which

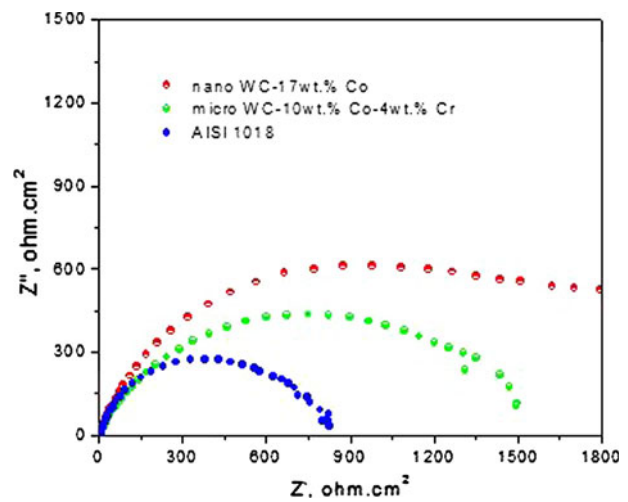


Fig. 10—Nyquist diagrams of engineered WC-17Co, microcrystalline WC-10Co-4Cr coatings, and uncoated carbon steel in 3.5 wt pct NaCl solution.

Table IV. EIS Data

Specimen	$R_s, \Omega\text{-cm}^2$	$Q, \text{F/cm}^2$	n	$R_t, \Omega\text{-cm}^2$
AISI 1018 steel	2.915	9.24×10^{-5}	0.78	811.5
Microcrystalline WC-10Co-4Cr	2.564	2.21×10^{-5}	0.72	1463
Near-nanocrystalline WC-17Co	3.72	8.74×10^{-5}	0.78	1919

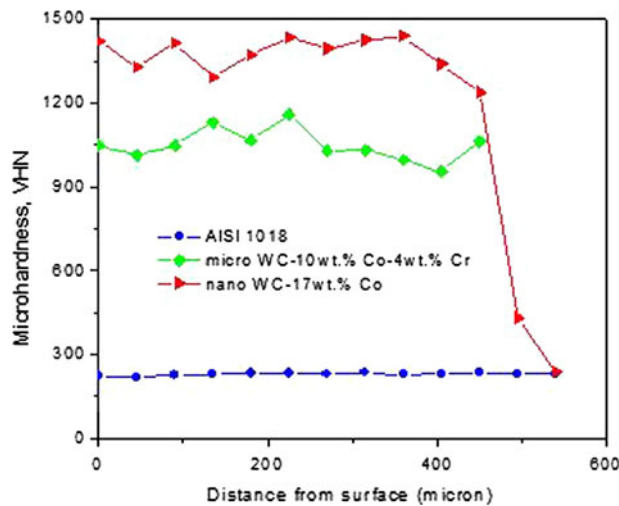


Fig. 11—Comparison of microhardness values as a function of depth through engineered WC-17Co, microcrystalline WC-10Co-4Cr coatings, and uncoated carbon steel.

represents the corrosion rate, increases for both coated surfaces. This indicates that the coatings inhibit the corrosion of carbon steel. However, the shape of the impedance spectra does not change, which suggests that the coatings do not change the electrochemical mechanism. Any change in electrochemical mechanisms would have been seen as two EIS semicircles in the test result. To quantify the electrochemical parameters, an equivalent circuit $R_s(R_tQ)$ was used for fitting EIS data. In the equivalent circuit, R_s is the solution resistance, Q is the constant phase element, an R_t is the charge transfer resistance. The values of the impedance parameters are listed in Table IV.

From the data, it can be seen that the charge transfer resistance, R_t , of the coated electrodes, which represents the reaction rate, is higher than that of the uncoated electrode. Furthermore, the largest charge transfer resistance is given for the engineered near-nanocrystalline WC-17Co coating, which indicates that the engineered coating decreases the corrosion of the substrate significantly. It is also noted that the microcrystalline WC-10Co-4Cr coating is close to Warburg impedance and not capacitive. These results are consistent with those of the polarization curve measurements recorded in Figure 7.

C. Vickers Microhardness

The change in microhardness as a function of depth through the steel substrate and the coating surfaces is shown in Figure 11. A uniform hardness profile through

Table V. Comparison of Hardness and Wear Rate of Coated and Uncoated Steel Substrate

Specimen	Vickers Microhardness, VHN	Wear Rate, mm^3/Nm
AISI 1018 steel	230	0.17
Microcrystalline WC-10Co-4Cr	1048	0.009
Near-nanocrystalline WC-17Co	1440	0.0065

the entire thickness of the coatings confirms the homogeneity of both microcrystalline WC-10Co-4Cr and engineered near-nanocrystalline WC-17Co coatings. The microhardness values were significantly higher for coatings when compared with those of the carbon steel and are given in Table V. A hardness increase of more than 25 pct for the engineered near-nanocrystalline over the microcrystalline coating was obtained. This increase in hardness with a change in near-nanocrystalline to microcrystalline grain structure can be attributed to the higher density of the near-nanocrystalline coating, as well as the established Hall–Patch relationship in which the yield stress increases as the grain size decreases.

D. Abrasive Wear Resistance

A two-body abrasive wear test was performed in order to compare abrasive wear resistance between the coated and uncoated steel, per ASTM G133-05 standard test protocol. The wear graphs are shown in Figure 12.

It is seen that the best wear resistance was recorded for the engineered near-nanocrystalline coating followed by the traditional microcrystalline coating. Comparing the steady-state wear rates for the uncoated AISI 1018 substrate and coated specimens, a value of $0.17 \text{ mm}^3/\text{Nm}$ was obtained for the carbon steel AISI 1018. The wear rate of WC-10Co-4Cr coating was extremely low with a value of $0.009 \text{ mm}^3/\text{Nm}$, which was approximately 19 times more wear resistant than the AISI 1018 substrate. Finally, the lowest wear rate was recorded for the near-nanocrystalline WC-17Co coating (Table V). The increase in wear resistance of the near-nanocrystalline coating over the microcrystalline coating can be attributed directly to the higher hardness value of the near-nanocrystalline coating. Furthermore, the more compact near-nanocrystalline structure, which is free of microporosity, will increase the wear life of the coating because the presence of porosity can lead to stress concentration around pores and delamination failure of the coating.

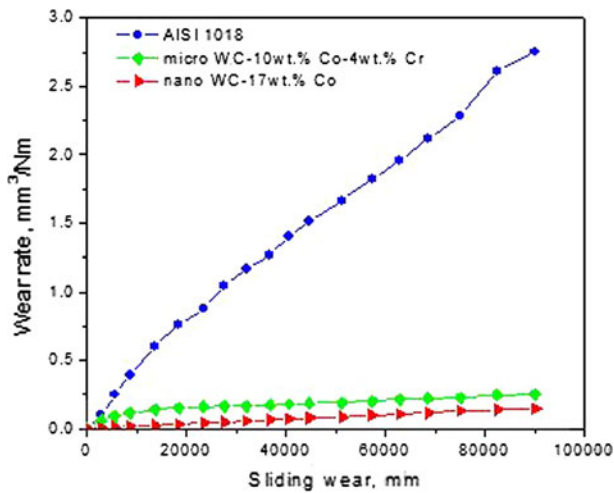


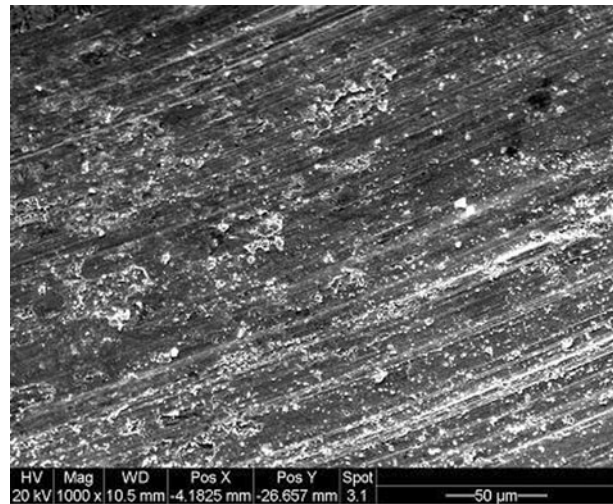
Fig. 12—Wear rate as a function of sliding distance for engineered WC-17Co, microcrystalline WC-10Co-4Cr coatings, and uncoated carbon steel.

Figure 13 shows the scanning electron micrographs taken from the abrasive wear tracks of the microcrystalline WC-10Co-4Cr and near-nanocrystalline WC-17Co coatings. In Figure 13(b), the near-nanocrystalline coating exhibits microcutting and plastic deformation of the surface with fine wear debris. The microcrystalline coating (Figure 13(a)), on the other hand, shows less plastic deformation, but a greater extent of brittle fracture within the wear track. The wear debris was larger and angular in morphology. These differences in material removal from the coatings suggest a distinct difference in wear mechanisms between the two coatings.

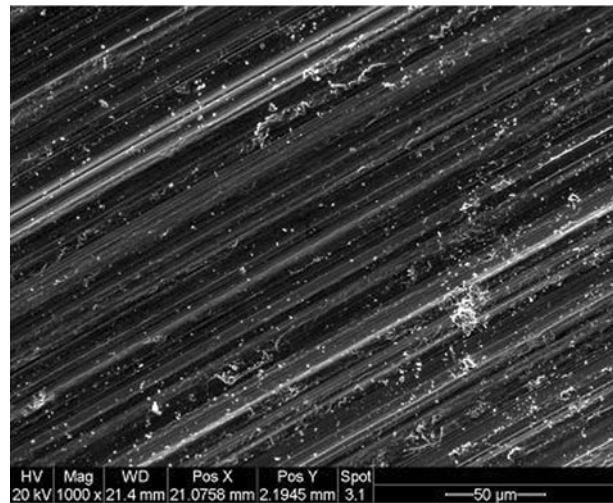
IV. CONCLUSIONS

In this study, the corrosion and wear-resistant behavior of the HVOF-sprayed near-nanocrystalline WC-17Co and industry standard conventional microcrystalline WC-10Co-4Cr coatings were compared. The following conclusions are drawn.

1. The duplex Co coated near-nanocrystalline WC-17Co powder prevented significant decarburization of the WC dispersion. Noticeable decarburization of the conventional microcrystalline WC-10Co-4Cr powder was recorded.
2. Potentiodynamic tests showed that the anodic polarization curves shift to a more positive potential for the near-nanocrystalline WC-17Co coating compared to the microcrystalline WC-10Co-4Cr coating.
3. The microcrystalline WC-10Co-4Cr and near-nanocrystalline WC-17Co coatings showed higher charge transfer resistance, which in turn indicated the lower corrosion rate, than that of the uncoated AISI 1018 steel. Comparing this performance between



(a)



(b)

Fig. 13—SEM micrographs showing (a) microcrystalline WC-10Co-4Cr and (b) near-nanocrystalline WC-17Co coating sliding wear tracks.

the two coatings, the corrosion rate in the near-nanocrystalline WC-17Co coating was smaller.

4. The near-nanocrystalline WC-17Co coating showed a 30 pct improvement in the abrasive wear resistance over that of the microcrystalline WC-10Co-4Cr coating. This increase in wear resistance of the near-nanocrystalline coating was attributed to an increase in the microhardness and the absence of microporosity in the coating.

ACKNOWLEDGMENTS

The authors thank Dr. G.A. Zhang (Corrosion and Pipeline Engineering Research Group, University of Calgary) for his assistance with corrosion testing. The financial support provided by the Natural Sciences and Engineering Research Council of Canada (NSERC) is gratefully acknowledged.

REFERENCES

1. G.E. Kim: in *Nanostructured Materials: Processing, Properties, and Applications*, C.C. Koch, ed., William Andrew Publishing, New York, NY, 2007, 2nd ed., pp. 91–118.
2. C. Monticelli, A. Frignani, and F. Zucchi: *Corros. Sci.*, 2004, vol. 46, pp. 1225–37.
3. J.A. Picas, A. Forn, A. Igartua, and G. Mendoza: *Surf. Coat. Technol.*, 2003, vols. 174–175, pp. 1095–1100.
4. J. Larsen-Basse, C.M. Perrott, and P.M. Robinson: *Mater. Sci. Eng.*, 1974, vol. 13, pp. 83–91.
5. H.M. Hawthorne, B. Arsenault, J.P. Immarigeon, J.G. Legoux, and V.R. Parameswaran: *Wear*, 1999, vols. 225–229, pp. 825–34.
6. M.G. Gee, A. Gant, and B. Roebuck: *Wear*, 2007, vol. 263, pp. 137–48.
7. M. Nganbe, T.I. Khan, and L.B. Glesnek: *Proc. Materials Technology in Mechanical Engineering*, Canadian Society for Mechanical Engineering (CSME) Forum, Kananaskis, AB, 2006, p. 13.
8. H.J.C. Voorwald, R.C. Souza, W.L. Pigatin, and M.O.H. Cioffi: *Surf. Coat. Technol.*, 2005, vol. 190, pp. 155–64.
9. G.C. Saha, T.I. Khan, and L.B. Glesnek: *J. Nanosci. Nanotechnol.*, 2009, vol. 9, pp. 4316–23.
10. D.A. Stewart, P.H. Shipway, and D.G. McCartney: *Acta Mater.*, 2000, vol. 48, pp. 1593–604.
11. B.K. Kear and L.E. McCandlish: *Nanostruct. Mater.*, 1993, vol. 3, pp. 19–30.
12. J. He, M. Ice, S. Dallek, and E.J. Lavernia: *Metall. Mater. Trans. A*, 2000, vol. 31A, pp. 541–53.
13. B.K. Kear and L.E. McCandlish: *Nanostruct. Mater.*, 1992, vol. 1, pp. 119–24.
14. J. He and J.M. Schoenung: *Surf. Coat. Technol.*, 2002, vol. 157, pp. 72–79.
15. L.E. McCandlish, B. Kear, and B.K. Kim: *J. Mater. Sci. Technol.*, 1990, vol. 6, pp. 953–60.
16. K. Jia, T.E. Fischer, and G. Gallois: *J. Nanostruct. Mater.*, 1998, vol. 10, pp. 875–91.
17. K. Jia and T.E. Fischer: *Wear*, 1996, vol. 200, pp. 206–14.
18. K. Jia and T.E. Fischer: *Wear*, 1997, vols. 203–204, pp. 310–18.
19. S. Usmani and S. Sampath: *Tribol. Trans.*, 1997, vol. 40, pp. 470–78.
20. D.A. Stewart, P.H. Shipway, and D.G. McCartney: *Wear*, 1999, vols. 225–229, pp. 789–98.
21. Y. Qiao, Y.R. Liu, and T.E. Fischer: *J. Thermal Spray Technol.*, 2001, vol. 10, pp. 118–25.
22. A.H. Dent, S. DePalo, and S. Sampath: *J. Thermal Spray Technol.*, 2002, vol. 11, pp. 551–58.
23. R. Valiev: *Nature*, 2002, vol. 419, pp. 887–88.
24. Y. Qiao, T.E. Fischer, and A. Dent: *Surf. Coat. Technol.*, 2003, vol. 172, pp. 24–41.
25. H. Chen, G.Q. Gou, M.J. Tu, and Y. Liu: *Surf. Eng.*, 2009, vol. 25, pp. 502–06.
26. T.I. Khan, G.C. Saha, and L.B. Glesnek: *Surf. Eng.*, 2010, in press.
27. A. Matthews, S. Franklin, and K. Holmberg: *J. Phys. D: Appl. Phys.*, 2007, vol. 40, pp. 5463–75.
28. P.G. Engleman: MesoCoat Inc., Euclid, OH, unpublished research, 2009.
29. J.M. Perry, A. Neville, and T. Hodgkiess: *J. Thermal Spray Technol.*, 2002, vol. 11, pp. 536–41.
30. B.H. Kear, R.K. Sadangi, M. Jain, R. Yao, Z. Kalman, G. Skandan, and W.E. Mayo: *J. Thermal Spray Technol.*, 2000, vol. 9, pp. 399–406.
31. J.M. Guilemany, S. Dosta, J. Nin, and J.R. Miguel: *Surf. Coat. Technol.*, 2006, vol. 201, pp. 1180–90.